Progress In Electromagnetics Research, Vol. 112, 273–298, 2011

TWO L-SHAPED ARRAY-BASED 2-D DOAS ESTIMATION IN THE PRESENCE OF MUTUAL COUPLING

J. Liang and D. Liu

School of Automation & Information Engineering
Xi'an University of Technology
Xi'an, China

Abstract—Recent research on the array geometrical configuration shows that the two L-shaped array (TLSA) has a lower Cramer-Rao Low-Bound (CRLB) of two-dimensional (2-D) directions-of-arrival (DOAs) estimation than other array configurations. However, in this array configuration, there are some problems to note: i) three electric angles are independently obtained from three uniformly linear subarrays on three axes, so they must be matched before solving elevation and azimuth angles from them; ii) Similar to other array geometries, the effect of mutual coupling in the TLSA on the estimation performance cannot be ignored; and iii) the conventional elevation estimators may encounter estimation failure.

In this paper, we develop a new TLSA-based 2-D DOAs estimation algorithm. The key points of this paper are: i) using some particularly selecting matrices, a trilinear model is constructed to compensate the effect of mutual coupling on three subarrays. In addition, the steering vector is restored using the trilinear alternating least square method; ii) 2-D DOAs are estimated from the properly chosen elements of the restored steering vector to avoid pairing parameters and the severe performance degradation resulted from the failure in pairing; and iii) a new elevation estimator is designed to avoid estimation failure. Simulation results are presented to validate the performance of the proposed method.

Received 17 July 2010, Accepted 6 September 2010, Scheduled 20 January 2011
Corresponding author: J. Liang (liangjunli@xaut.edu.cn).

1. INTRODUCTION

Estimation of two-dimensional (2-D) directions-of -arrival (DOAs) plays an important role in array signal processing fields such as mobile communication, radar, sonar, and radio astronomy [1–5]. This issue can be divided into several topics: i) array geometry [3–8]; ii) estimation method [9–12]; iii) match of separately obtained estimations [13–26] (Note that parameter match operation is a key step in the 2-D DOAs estimation problem, and the failure in pairing will cause severe performance degradation); iv) the mutual coupling effect among multiple sensors can not be ignored since it may cause severe performance degradation [27–37], as shown in the linear array [32, 35], the circular array [27–29], the rectangular array [30], and the hexagon array [31]; and v) the estimation failure problem, i.e., the elevation estimator $\hat{\alpha}_l = \text{asin}(\sqrt{\hat{\gamma}_l^2 + \hat{\phi}_l^2}\lambda/(2\pi d))$ may fail since the estimation of $\{\gamma_l, \phi_l\}$ causes $\sqrt{\hat{\gamma}_l^2 + \hat{\phi}_l^2}\lambda/(2\pi d) > 1$, especially when elevation angle is between 70° and 90° that is often encountered in mobile communication, as shown in [8, 16].

Comparing with the parallel uniform linear array, the rectangular array, and the circular array, the L-shaped array (LSA) [6–8, 13–15, 25], especially two L-shaped array (TLSA) [6, 8], has received a significant amount of attention due to some advantages in low CRLB [6] and independent implementation of multiple uniform linear subarrays. Tayem and Kwon proposed a TLSA-based propagator method for 2-D DOAs estimation [8]. However, it cannot provide a reasonable mechanism on matching the separately obtained estimations [13, 15] (i.e., the third topic of the above-mentioned estimation issue). Besides, it does not consider the mutual coupling effect among multiple sensors (i.e., the fourth topic of the above-mentioned estimation issue) [8].

In this paper, we develop a new TLSA-based 2-D DOAs estimation algorithm. The key points of this paper are: i) using some particularly selecting matrices, a trilinear model is constructed to compensate the effect of mutual coupling on three subarrays. In addition, the steering vector is restored using the trilinear alternating least square method; ii) 2-D DOAs are estimated from the properly chosen elements of the restored steering vector to avoid pairing parameters and the severe performance degradation resulted from the failure in pairing; and iii) a new elevation estimator is designed to avoid estimation failure.

In fact, Sidiropoulos et al. have developed a rectangular array-based 2-D DOAs estimation method using the trilinear model [40]. We stress that there are some obvious differences between the method in [40] and the proposed algorithm except the common use of the

trilinear model: i) difference array configurations. Note that there exists obvious rotational invariance property in the rectangular array configuration to form a trilinear model [40]. However, the proposed algorithm forms the trilinear model from three orthogonal subarrays (without any commonly rotational invariance characteristics) using the eigenvalue decomposition operation, pseudo-inverse operation, and some particularly selecting matrices; ii) on the estimation failure problem. The method in [40] encountered the estimation failure from the elevation estimator $\hat{\alpha}_l = \text{asin}(\sqrt{\hat{\gamma}_l^2 + \hat{\phi}_l^2}\lambda/(2\pi d))$. However, the proposed algorithm uses the two L-shaped array and three electric angles to form a new estimator, thus avoiding estimation failure; and iii) the proposed algorithm considers the effect of mutual coupling, which is not considered in [40].

The rest of this paper is organized as follows. The signal model is introduced in Section 2. A new algorithm is developed in Section 3. Simulation results are presented in Section 4. Conclusions are drawn in Section 5.

2. SIGNAL MODEL AND TRILINEAR MODEL

2.1. Signal Model

Consider two L-shaped array (TLSA) of $3M+1$ omnidirectional sensors with element spacing d shown in Fig. 1 [6, 8]. The element placed at the origin is set for the referencing point. The array consists of two

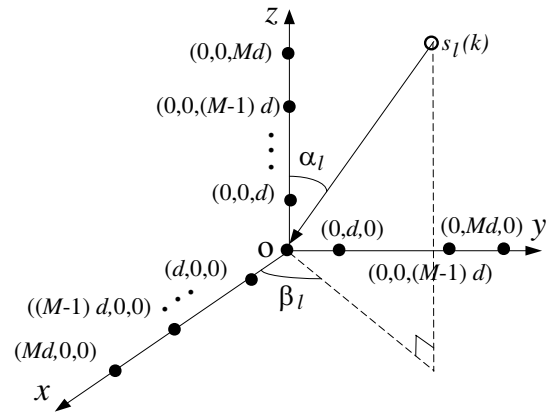

Figure 1. Two L-shaped array configuration.

L-shaped subarrays, one being in the x-z plane and another being in the y-z plane. Assume that L far-field narrowband sources impinging on the TLSA. Let α_l and β_l be the elevation and azimuth angles of the lth source, and thus the wave vector $\boldsymbol{\kappa}_l$ containing DOA information can be defined as [16]

$$\boldsymbol{\kappa}_l = [\sin\alpha_l \cos\beta_l, \sin\alpha_l \sin\beta_l, \cos\alpha_l], \quad l = 1, \ldots, L. \tag{1}$$

In the rest of this paper, the (m, p, q)th sensor stands for the element with coordinates (md, pd, qd), where $(m, p, q) \in \{(1,0,0), \ldots, (M,0,0), (0,0,0), (0,1,0), \ldots, (0,M,0), (0,0,1), \ldots, (0,0,M)\}$. Let $\mathbf{C}$ denotes the mutual coupling matrix, thus the output of the TLSA can be expressed as:

$$\mathbf{r}(k) = \mathbf{CAs}(k) + \mathbf{n}(k) = \sum_{l=1}^{L} \mathbf{Ca}(\gamma_l, \phi_l, \vartheta_l) s_l(k) + \mathbf{n}(k) \quad k = 0, \ldots, K-1, \tag{2}$$

where $\mathbf{r}(k)$, $\mathbf{A}$, $\mathbf{s}(k)$, and $\mathbf{n}(k)$ stand for the received signal vector, the ideal steering matrix, the source signal vector, and the noise vector, respectively. They can be expressed as

$$\begin{aligned} \mathbf{r}(k) &= [r_{1,0,0}(k) \ldots r_{M,0,0}(k)\ r_{0,0,0}(k) r_{0,1,0}(k) \ldots r_{0,M,0}(k) \\ &\quad r_{0,0,1}(k) \ldots\ r_{0,0,M}(k)], \end{aligned} \tag{3}$$

$$\mathbf{A} = [\mathbf{a}(\gamma_1, \phi_1, \vartheta_1) \ldots \mathbf{a}(\gamma_l, \phi_l, \vartheta_l) \ldots \mathbf{a}(\gamma_L, \phi_L, \vartheta_L)], \tag{4}$$

$$\mathbf{s}(k) = [s_1(k), \ldots, s_l(k), \ldots, s_L(k)]^T, \tag{5}$$

$$\mathbf{a}(\gamma_l, \phi_l, \vartheta_l) = \left[e^{j\gamma_l} \ldots e^{jM\gamma_l}\ 1\ e^{j\phi_l} \ldots e^{jM\phi_l}\ e^{j\vartheta_l} \ldots e^{jM\vartheta_l}\right]^T, \tag{6}$$

and

$$\begin{aligned} \mathbf{n}(k) &= [n_{1,0,0}(k)\ \ldots n_{M,0,0}(k)\ n_{0,0,0}(k)\ n_{0,1,0}(k)\ \ldots\ n_{0,M,0}(k) \\ &\quad n_{0,0,1}(k)\ \ldots\ n_{0,0,M}(k)]^T, \end{aligned} \tag{7}$$

and three electric angles γ_l, ϕ_l, and ϑ_l (being functions of elevation angle α_l and azimuth angle β_l):

$$\gamma_l = -2\pi d \sin\alpha_l \cos\beta_l / \lambda, \tag{8}$$

$$\phi_l = -2\pi d \sin\alpha_l \sin\beta_l / \lambda, \tag{9}$$

and

$$\vartheta_l = -2\pi d \cos\alpha_l / \lambda. \tag{10}$$

References [30, 36, 37] show that the coupling between neighboring elements with the same interspace is almost the same, and the magnitude of the mutual coupling coefficient between two distant elements is so small that it can be approximated to zero. Thus, it is often sufficient

to consider the coupling model with just a few nonzero coefficients and a banded symmetric Toeplitz matrix can be used as the model for the mutual coupling coefficients. Similar to [30, 36, 37], this paper assumes that the (m, p, q)th sensor is only affected by the sensors inside or on the related sphere centered at (md, pd, qd) and with radius $\sqrt{2}d$ (Although we assume each sensor is affected by those within the range $\sqrt{2}d$ in this paper, the proposed algorithm can be tuned to be applicable to other ranges), i.e., the (m, p, q)th sensor is affected by the $(m + \Delta m, p + \Delta p, q + \Delta q)$th sensor if and only if $\Delta m, \Delta p, \Delta q \in \{-1, 0, 1\}$, $\sqrt{(\Delta m)^2 + (\Delta p)^2 + (\Delta q)^2} < 2$, and $(m + \Delta m, p + \Delta p, q + \Delta q) \in \{(1, 0, 0), \ldots, (M, 0, 0), (0, 0, 0), (0, 1, 0), \ldots, (0, M, 0), (0, 0, 1), \ldots, (0, 0, M)\}$. For example, the $(0, 1, 0)$th sensor is affected by the $(0, 2, 0)$th, $(0, 0, 0)$th, $(1, 0, 0)$th, and $(0, 0, 1)$th sensors, whereas the $(0, 2, 0)$th sensor is affected by the $(0, 1, 0)$th, and $(0, 3, 0)$th sensors. Note that when $m \geq 2$, the $(m, 0, 0)$th sensor is affected only by the $(m+1, 0, 0)$th and $(m - 1, 0, 0)$th sensors, and no longer affected by other sensors. The similar case holds for $q \geq 2$ or $p \geq 2$. The mutual coupling matrix $\mathbf{C}$ can be represented as:

$$\mathbf{C} = \begin{bmatrix} \mathbf{D}_1 & \mathbf{d}_3 & \mathbf{D}_2 & \mathbf{D}_2 \\ \mathbf{d}_3^T & 1 & \mathbf{d}_3^T & \mathbf{d}_3^T \\ \mathbf{D}_2 & \mathbf{d}_3 & \mathbf{D}_1 & \mathbf{D}_2 \\ \mathbf{D}_2 & \mathbf{d}_3 & \mathbf{D}_2 & \mathbf{D}_1 \end{bmatrix}, \tag{11}$$

where the $M \times M$-dimensional mutual coupling matrix $\mathbf{D}_1$ within any subarray is a banded symmetric Toeplitz matrix, i.e.,

$$\mathbf{D}_1 = \begin{bmatrix} 1 & c_1 & 0 & 0 & \ldots & 0 \\ c_1 & 1 & c_1 & 0 & \ldots & 0 \\ 0 & c_1 & 1 & c_1 & \ldots & 0 \\ \vdots & \ddots & \ddots & \ddots & \ddots & \vdots \\ 0 & \ldots & 0 & c_1 & 1 & c_1 \\ 0 & \ldots & 0 & 0 & c_1 & 1 \end{bmatrix}_{M \times M}, \tag{12}$$

$$\mathbf{d}_3 = \begin{bmatrix} c_1 & \underbrace{\mathbf{0}}_{M-1} \end{bmatrix}, \tag{13}$$

and the $M \times M$-dimensional mutual coupling matrix $\mathbf{D}_2$ between two subarrays can be represented as:

$$\mathbf{D}_2 = \begin{bmatrix} c_2 & \underbrace{\mathbf{0}}_{1\times(M-1)} \\ \underbrace{\mathbf{0}}_{(M-1)\times 1} & \underbrace{\mathbf{0}}_{(M-1)\times(M-1)} \end{bmatrix}_{M \times M}. \tag{14}$$

The objective of this paper is to jointly estimate elevation angle α_l and azimuth angle β_l for $l = 1, \ldots, L$. Throughout the paper, the following hypotheses are assumed to hold:

1) The source signals are uncorrelated ones;
2) The sensor noise is additive white Gaussian one with zero-mean and independent of the source signals;
3) For unique estimation, we require $L < M - 2$;
4) Element spacing d is not larger than half wavelength.

2.2. Trilinear Model [38–42]

Definition 1: Consider a $(I \times J \times K)$-dimensional three-way array (TWA) $\mathbf{X} = (\mathbf{D} \otimes \mathbf{H})\mathbf{W}^T$ ($\otimes$ stands for *Kronecker* product) with typical element $x_{i,j,k}$ and the F-component trilinear decomposition

$$x_{i,j,k} = \sum_{f=1}^{F} d_{i,f} h_{j,f} w_{k,f}, \tag{15}$$

for $i = 1, \ldots, I$, $j = 1, \ldots, J$, and $k = 1, \ldots, K$, where $d_{i,f}$ represents the (i, f)th element of $(I \times F)$-dimensional matrix $\mathbf{D}$. Similarly, $h_{j,f}$ and $w_{k,f}$ stand for the (j, f)th and (k, f)th elements of $(J \times F)$ and $(K \times F)$-dimensional matrices $\mathbf{H}$ and $\mathbf{W}$, respectively. Eq. (15) expresses $x_{i,j,k}$ as a sum of F rank-1 triple products; it is known as trilinear analysis of $x_{i,j,k}$.

Definition 2: Let $\mathrm{diag}_i(\mathbf{D})$ denotes a diagonal matrix composed of the ith row of matrix $\mathbf{D}$, and $\mathrm{diag}^{-1}(\mathbf{\Lambda})$ stands for a row vector made up of the diagonal elements of diagonal matrix $\mathbf{\Lambda}$.

In a compact form, $\mathbf{X}$ can be expressed in terms of its 2-D slice $\mathbf{X}_i$ ($(J \times K)$-dimensional matrix, i.e., $\mathbf{X}_i = [x_{i,:,:}]$) as:

$$\mathbf{X}_i = \mathbf{H}\mathrm{diag}_i(\mathbf{D})\mathbf{W}^T, \quad i = 1, \ldots, I. \tag{16}$$

Under certain conditions, $\mathbf{X}$ can be decomposed uniquely into matrices $\mathbf{D}$, $\mathbf{H}$, and $\mathbf{W}$. These conditions are based on the notion of *Kruskal*-rank.

Definition 3: The *Kruskal* rank (or k-rank) of matrix $\mathbf{D}$ is $k_{\mathbf{D}}$ if and only if every $k_{\mathbf{D}}$ columns of $\mathbf{D}$ are linearly independent and either $\mathbf{D}$ has $k_{\mathbf{D}}$ columns or $\mathbf{D}$ contains a set of $k_{\mathbf{D}} + 1$ linearly dependent columns. Note that *Kruskal* rank is always less than or equal to the conventional matrix rank. If $\mathbf{D}$ is of full column rank, then it is also of full k-rank [40].

Theorem 1 [40, 41]: Let $\mathbf{X}_i$ be defined as in Eq. (16). $\mathbf{D}$, $\mathbf{H}$, and $\mathbf{W}$ can be recovered uniquely up to permutation and scaling ambiguity,

irrespective of whether the elements of $\mathbf{X}$ are real values or complex ones, as long as

$$k_{\mathbf{D}} + k_{\mathbf{H}} + k_{\mathbf{W}} \geq 2F + 2, \tag{17}$$

which is the well-known Kruskal's condition. In fact, this result holds for one source case, that is, $L = 1$, irrespective of ***Theorem*** 1, as long as $\mathbf{X}$ does not contain an identically zero 2D slice along any dimension.

3. PROPOSED ALGORITHM

3.1. Analysis of the TLSA Configuration

For the TLSA configuration, a feasible solution is to firstly estimate electric angles $\{\gamma_l, \phi_l, \vartheta_l\}$ then to solve $\{\alpha_l, \beta_l\}$ from $\{\gamma_l, \phi_l, \vartheta_l\}$ (see Eqs. (6), (8)–(10) for details) due to the fact that $\{\gamma_l, \phi_l, \vartheta_l\}$ rather than $\{\alpha_l, \beta_l\}$ are more easily calculated from $\mathbf{r}(k)$. Although $\{\gamma_{x1}, \gamma_{x2}, \ldots, \gamma_{xL}\}$, $\{\phi_{y1}, \phi_{y2}, \ldots, \phi_{yL}\}$, and $\{\vartheta_{z1}, \vartheta_{z2}, \ldots, \vartheta_{zL}\}$ can be calculated from three uniform linear subarrays independently, the pairing problem becomes evident since three permutations $\{x1, x2, \ldots, xL\}$, $\{y1, y2, \ldots, yL\}$, $\{z1, z2, \ldots, zL\}$ of $\{1, 2, \ldots, L\}$ may be different from each other [13, 15]. Furthermore, the effect of mutual coupling on the DOA estimation performance can not be ignored. Although many algorithms have been developed for one-dimensional DOA estimation in the presence of mutual coupling, there are few researches addressing 2-D case, especially for the L-shaped array. Moreover, some researches show that the elevation estimation $\hat{\alpha}_l = \text{asin}(\sqrt{\hat{\gamma}_l^2 + \hat{\phi}_l^2}\lambda/(2\pi d))$ may fail since the estimation of $\{\gamma_l, \phi_l\}$ may cause $\sqrt{\hat{\gamma}_l^2 + \hat{\phi}_l^2}\lambda/(2\pi d) > 1$, especially when elevation angles lie within 70° and 90°, which is often encountered in mobile communication [8, 16].

To solve these problems, we consider: i) the three electric angles $\{\gamma_l, \phi_l, \vartheta_l\}$ must be correctly matched so that 2-D DOAs $\{\alpha_l, \beta_l\}$ can be solved from Eqs. (8)–(10). In this work, we estimate the three electric angles from the recovered steering vector to avoid the failure in pairing; ii) in the TLSA configuration, three electric angles rather than two ones can be used for solving elevation and azimuth angles, which can enhance the flexibility of estimators and avoid estimation failure [8]. In this work, we design a new elevation angle estimator to avoid estimation failure [16] using the three electric angles; and iii) using some particularly selecting matrices, a trilinear model is constructed to compensate the effect of mutual coupling on three subarrays.

3.2. Analysis the Steering Vector in the Presence of Mutual Coupling

To compensate the effect of mutual coupling, we set the $(0,0,0)$th, $(0,1,0)$th, $(1,0,0)$th, $(0,0,1)$th, $(M,0,0)$th, $(0,0,M)$th, and $(0,M,0)$th sensors as auxiliary ones.

Define the first $(M-2)\times(3M+1)$-dimensional selecting matrix:

$$\mathbf{W}_1 = \left[\underbrace{0}_{(M-2)\times 1} \quad \underbrace{\mathbf{I}}_{(M-2)\times(M-2)} \quad \underbrace{0}_{(M-2)\times(2M+2)} \right], \tag{18}$$

and the output of the $\{(2,0,0),(3,0,0),\ldots,(M-1,0,0)\}$th sensors on the x-axis can be represented as:

$$\begin{aligned}\mathbf{W}_1\mathbf{r}(k) &= \mathbf{W}_1\left(\mathbf{CAs}(k)+\mathbf{n}(k)\right)=\sum_{l=1}^{L}\mathbf{W}_1\mathbf{Ca}(\gamma_l,\phi_l,\vartheta_l)s_l(k)+\mathbf{W}_1\mathbf{n}(k)\\ &= \left[r_{2,0,0}(k)\ r_{3,0,0}(k)\ldots r_{M-1,0,0}(k)\right]^T,\end{aligned} \tag{19}$$

where

$$\begin{aligned}\mathbf{W}_1\mathbf{Ca}(\gamma_l,\phi_l,\vartheta_l) &= \begin{bmatrix} c_1e^{j\gamma_l}+e^{j2\gamma_l}+c_1e^{j3\gamma_l} \\ c_1e^{j2\gamma_l}+e^{j3\gamma_l}+c_1e^{j4\gamma_l} \\ \vdots \\ c_1e^{j(M-3)\gamma_l}+e^{j(M-2)\gamma_l}+c_1e^{j(M-1)\gamma_l} \\ c_1e^{j(M-2)\gamma_l}+e^{j(M-1)\gamma_l}+c_1e^{jM\gamma_l} \end{bmatrix}\\ &= \left(c_1e^{j\gamma_l}+e^{j2\gamma_l}+c_1e^{j3\gamma_l}\right)\begin{bmatrix} 1 \\ e^{j\gamma_l} \\ \vdots \\ e^{j(M-4)\gamma_l} \\ e^{j(M-3)\gamma_l} \end{bmatrix} = \xi(\gamma_l)\begin{bmatrix} 1 \\ e^{j\gamma_l} \\ \vdots \\ e^{j(M-4)\gamma_l} \\ e^{j(M-3)\gamma_l} \end{bmatrix}\end{aligned} \tag{20}$$

and $\xi(\gamma_l)=(c_1e^{j\gamma_l}+e^{j2\gamma_l}+c_1e^{j3\gamma_l})$, which can be considered as a disturbance on the steering vector $\begin{bmatrix} 1 & e^{j\gamma_l} & \ldots & e^{j(M-4)\gamma_l} & e^{j(M-3)\gamma_l} \end{bmatrix}^T$ of virtual uniform linear array. From Eq. (17), we can see that although the $\{(2,0,0),(3,0,0),\ldots,(M-1,0,0)\}$th sensors are affected by the mutual coupling, there are still linear phase delay characteristics among these sensors.

Similarly, we define the second $(M-2)\times(3M+1)$-dimensional selecting matrix:

$$\mathbf{W}_2 = \left[\underbrace{0}_{(M-2)\times(M+2)} \quad \underbrace{\mathbf{I}}_{(M-2)\times(M-2)} \quad \underbrace{0}_{(M-2)\times(M+1)} \right] \tag{21}$$

and the output of the $\{(0,2,0),(0,3,0),\ldots,(0,M-1,0)\}$th sensors on the y-axis can be represented as:

$$\mathbf{W}_2\mathbf{r}(k)=\mathbf{W}_2\left(\mathbf{CAs}(k)+\mathbf{n}(k)\right)=\sum_{l=1}^{L}\mathbf{W}_2\mathbf{Ca}(\gamma_l,\phi_l,\vartheta_l)s_l(k)+\mathbf{W}_2\mathbf{n}(k)$$
$$=[r_{0,2,0}(k)\ r_{0,3,0}(k)\ldots r_{0,M-1,0}(k)]^T \tag{22}$$

where

$$\mathbf{W}_2\mathbf{Ca}(\gamma_l,\phi_l,\vartheta_l)=\begin{bmatrix} c_1e^{j\phi_l}+e^{j2\phi_l}+c_1e^{j3\phi_l} \\ c_1e^{j2\phi_l}+e^{j3\phi_l}+c_1e^{j4\phi_l} \\ \vdots \\ c_1e^{j(M-3)\phi_l}+e^{j(M-2)\phi_l}+c_1e^{j(M-1)\phi_l} \\ c_1e^{j(M-2)\phi_l}+e^{j(M-1)\phi_l}+c_1e^{jM\phi_l} \end{bmatrix}$$
$$=\left(c_1e^{j\phi_l}+e^{j2\phi_l}+c_1e^{j3\phi_l}\right)\begin{bmatrix} 1 \\ e^{j\phi_l} \\ \vdots \\ e^{j(M-4)\phi_l} \\ e^{j(M-3)\phi_l} \end{bmatrix}=\xi\left(\phi_l\right)\begin{bmatrix} 1 \\ e^{j\phi_l} \\ \vdots \\ e^{j(M-4)\phi_l} \\ e^{j(M-3)\phi_l} \end{bmatrix} \tag{23}$$

and $\xi(\phi_l)=\left(c_1e^{j\phi_l}+e^{j2\phi_l}+c_1e^{j3\phi_l}\right)$.

Define the third $(M-2)\times(3M+1)$-dimensional selecting matrix:

$$\mathbf{W}_3=\begin{bmatrix} \underbrace{0}_{(M-2)\times(2M+2)} & \underbrace{\mathbf{I}}_{(M-2)\times(M-2)} & \underbrace{0}_{(M-2)\times 1} \end{bmatrix} \tag{24}$$

and the output of the $\{(0,0,2),(0,0,3),\ldots,(0,0,M-1)\}$th sensors on the z-axis can be represented as:

$$\mathbf{W}_3\mathbf{r}(k)=\mathbf{W}_3\left(\mathbf{CAs}(k)+\mathbf{n}(k)\right)=\sum_{l=1}^{L}\mathbf{W}_3\mathbf{Ca}(\gamma_l,\phi_l,\vartheta_l)s_l(k)+\mathbf{W}_3\mathbf{n}(k)$$
$$=[\ r_{0,0,2}(k)\ r_{0,0,3}(k)\ldots r_{0,0,M-1}(k)\ ]^T \tag{25}$$

where

$$\mathbf{W}_3\mathbf{Ca}(\gamma_l,\phi_l,\vartheta_l)=\begin{bmatrix} c_1e^{j\vartheta_l}+e^{j2\vartheta_l}+c_1e^{j3\vartheta} \\ c_1e^{j2\vartheta}+e^{j3\vartheta_l}+c_1e^{j4\vartheta_l} \\ \vdots \\ c_1e^{j(M-3)\vartheta_l}+e^{j(M-2)\vartheta_l}+c_1e^{j(M-1)\vartheta_l} \\ c_1e^{j(M-2)\vartheta_l}+e^{j(M-1)\vartheta}+c_1e^{jM\vartheta_l} \end{bmatrix}$$

$$= \left(c_1 e^{j\vartheta_l} + e^{j2\vartheta_l} + c_1 e^{j3\vartheta_l}\right) \begin{bmatrix} 1 \\ e^{j\vartheta_l} \\ \vdots \\ e^{j(M-4)\vartheta_l} \\ e^{j(M-3)\vartheta_l} \end{bmatrix} = \xi(\vartheta_l) \begin{bmatrix} 1 \\ e^{j\vartheta_l} \\ \vdots \\ e^{j(M-4)\vartheta_l} \\ e^{j(M-3)\vartheta_l} \end{bmatrix} \quad (26)$$

and $\xi(\vartheta_l) = \left(c_1 e^{j\vartheta_l} + e^{j2\vartheta_l} + c_1 e^{j3\vartheta_l}\right)$.

Note that the disturbances of the three subarrays are different from each other, i.e., $\xi(\gamma_l) \neq \xi(\phi_l) \neq \xi(\vartheta_l)$, but there are linear phase delay characteristics among the partly sensors in each subarray.

3.3. Constructing a Trilinear Model that Can Compensating the Effect of Mutual Coupling

To develop a new joint estimation algorithm, we begin with the autocorrelation matrix of $\mathbf{r}(k)$, which can be expressed as:

$$\mathbf{R} = E\left[\mathbf{r}(k)\mathbf{r}^H(k)\right] = \mathbf{A}\mathbf{R}_s\mathbf{A}^H + \sigma_n^2\mathbf{I}_{3M+1}, \quad (27)$$

where $\mathbf{R}_s = E[\mathbf{s}(k)\mathbf{s}^H(k)]$. In the actual implementation, $\mathbf{R}$ must be estimated from available K snapshots, i.e., $\hat{\mathbf{R}} = \frac{1}{K}\sum_{k=0}^{K-1}\mathbf{r}(k)\mathbf{r}^H(k)$.

The eigenvalue decomposition (EVD) of $\hat{\mathbf{R}}$ yields

$$\begin{aligned} \hat{\mathbf{R}} &= \mathbf{U}\mathbf{V}\mathbf{U}^H = \mathbf{U}_s\mathbf{V}_s\mathbf{U}_s^H + \mathbf{U}_n\mathbf{V}_n\mathbf{U}_n^H \\ &= [\mathbf{u}_1, \ldots, \mathbf{u}_{3M+1}]\mathrm{diag}[v_1, \ldots, v_{3M+1}][\mathbf{u}_1, \ldots, \mathbf{u}_{3M+1}]^H \end{aligned} \quad (28)$$

where $\mathbf{V}$ is the diagonal matrix with the eigenvalues arranged as $v_1 \geq \ldots \geq v_L > v_{L+1} \geq \ldots \geq v_{3M+1}$, the diagonal matrix $\mathbf{V}_s \in R^{L\times L}$ is composed of eigenvalues $v_1, v_2, \ldots, v_L$; $\mathbf{U}_s \in C^{(3M+1)\times L}$, which spans the signal subspace of $\hat{\mathbf{R}}$, consists of the eigenvectors related to $v_1, v_2, \ldots, v_L$. Since the signal subspace $\mathbf{U}_s$ is equal to the range space of $\mathbf{CA}$, there must exist a unique invertible matrix $\mathbf{T}$, such that $\mathbf{U_s} = \mathbf{CAT}$.

Define an $(M-3)\times(3M+1)$-dimensional selecting matrices:

$$\mathbf{W}_{11} = \left[\underbrace{\mathbf{0}}_{(M-3)\times 1} \quad \underbrace{\mathbf{I}}_{(M-3)\times(M-3)} \quad \underbrace{\mathbf{0}}_{(M-3)\times(2M+3)}\right]. \quad (29)$$

Multiplying $\mathbf{W}_{11}$ on both sides of $\mathbf{U_s} = \mathbf{CAT}$ yields

$$\mathbf{W}_{11}\mathbf{U_s} = \mathbf{W}_{11}\mathbf{CAT} = \mathbf{B}(\gamma)\mathbf{\Omega}_1\mathbf{T}, \quad (30)$$

where

$$\mathbf{B}(\gamma) = [\mathbf{b}(\gamma_1)\dots\mathbf{b}(\gamma_l)\dots\mathbf{b}(\gamma_L)], \tag{31}$$

$$\mathbf{b}(\gamma_l) = \left[1\ e^{j\gamma_l}\dots e^{j(M-4)\gamma_l}\right]^T, \tag{32}$$

$$\mathbf{\Omega}_1 = \mathrm{diag}\left\{\xi(\gamma_1),\dots,\ \xi(\gamma_l),\dots,\xi(\gamma_L)\right\}. \tag{33}$$

Similar to $\mathbf{W}_{11}$, define five $(M-3)\times(3M+1)$-dimensional selecting matrices $\mathbf{W}_{12}$, $\mathbf{W}_{21}$, $\mathbf{W}_{22}$, $\mathbf{W}_{31}$, and $\mathbf{W}_{32}$ as follows:

$$\mathbf{W}_{12} = \left[\underbrace{\mathbf{0}}_{(M-3)\times 2}\ \underbrace{\mathbf{I}}_{(M-3)\times(M-3)}\ \underbrace{\mathbf{0}}_{(M-3)\times(2M+2)}\right] \tag{34}$$

$$\mathbf{W}_{21} = \left[\underbrace{\mathbf{0}}_{(M-3)\times(M+2)}\ \underbrace{\mathbf{I}}_{(M-3)\times(M-3)}\ \underbrace{\mathbf{0}}_{(M-3)\times(M+2)}\right] \tag{35}$$

$$\mathbf{W}_{22} = \left[\underbrace{\mathbf{0}}_{(M-3)\times(M+3)}\ \underbrace{\mathbf{I}}_{(M-3)\times(M-3)}\ \underbrace{\mathbf{0}}_{(M-3)\times(M+1)}\right] \tag{36}$$

$$\mathbf{W}_{31} = \left[\underbrace{\mathbf{0}}_{(M-3)\times(2M+2)}\ \underbrace{\mathbf{I}}_{(M-3)\times(M-3)}\ \underbrace{\mathbf{0}}_{(M-3)\times 2}\right] \tag{37}$$

$$\mathbf{W}_{32} = \left[\underbrace{\mathbf{0}}_{(M-3)\times(2M+3)}\ \underbrace{\mathbf{I}}_{(M-3)\times(M-3)}\ \underbrace{\mathbf{0}}_{(M-3)\times 1}\right] \tag{38}$$

Multiplying $\mathbf{W}_{12}$, $\mathbf{W}_{21}$, $\mathbf{W}_{22}$, $\mathbf{W}_{31}$, and $\mathbf{W}_{32}$ on both sides of $\mathbf{U_s} = \mathbf{CAT}$, respectively yields

$$\mathbf{W}_{12}\mathbf{U_s} = \mathbf{W}_{12}\mathbf{CAT} = \mathbf{B}(\gamma)\mathbf{\Omega}_1\mathbf{\Phi}_1\mathbf{T}, \tag{39}$$

$$\mathbf{W}_{21}\mathbf{U_s} = \mathbf{W}_{21}\mathbf{CAT} = \mathbf{B}(\phi)\mathbf{\Omega}_2\mathbf{T}, \tag{40}$$

$$\mathbf{W}_{22}\mathbf{U_s} = \mathbf{W}_{22}\mathbf{CAT} = \mathbf{B}(\phi)\mathbf{\Omega}_2\mathbf{\Phi}_2\mathbf{T}, \tag{41}$$

$$\mathbf{W}_{31}\mathbf{U_s} = \mathbf{W}_{31}\mathbf{CAT} = \mathbf{B}(\vartheta)\mathbf{\Omega}_3\mathbf{T}, \tag{42}$$

$$\mathbf{W}_{32}\mathbf{U_s} = \mathbf{W}_{32}\mathbf{CAT} = \mathbf{B}(\vartheta)\mathbf{\Omega}_3\mathbf{\Phi}_3\mathbf{T}, \tag{43}$$

where

$$\mathbf{B}(\phi) = [\mathbf{b}(\phi_1)\dots\mathbf{b}(\phi_l)\dots\mathbf{b}(\phi_L)], \tag{44}$$

$$\mathbf{b}(\phi_l) = \left[1\ e^{j\phi_l}\dots e^{j(M-4)\phi_l}\right]^T, \tag{45}$$

$$\mathbf{B}(\vartheta) = [\mathbf{b}(\vartheta_1)\dots\mathbf{b}(\vartheta_l)\dots\mathbf{b}(\vartheta_L)], \tag{46}$$

$$\mathbf{b}(\vartheta_l) = \left[1\ e^{j\vartheta_l} \dots e^{j(M-4)\vartheta_l}\right]^T, \tag{47}$$

$$\mathbf{\Omega}_2 = \text{diag}\left\{\xi(\phi_1), \dots, \xi(\phi_l), \dots, \xi(\phi_L)\right\}, \tag{48}$$

$$\mathbf{\Omega}_3 = \text{diag}\left\{\xi(\vartheta_1), \dots, \xi(\vartheta_l), \dots, \xi(\vartheta_L)\right\}, \tag{49}$$

$$\mathbf{\Phi}_1 = \text{diag}\left\{\left[e^{j\gamma_1}\ e^{j\gamma_2} \dots e^{j\gamma_L}\right]\right\}, \tag{50}$$

$$\mathbf{\Phi}_2 = \text{diag}\left\{\left[e^{j\phi_1}\ e^{j\phi_2} \dots e^{j\phi_L}\right]\right\}, \tag{51}$$

$$\mathbf{\Phi}_3 = \text{diag}\left\{\left[e^{j\vartheta_1}\ e^{j\vartheta_2} \dots e^{j\vartheta_L}\right]\right\}. \tag{52}$$

where diag $\{\cdot\}$ stands for a square diagonal matrix.

From equation pairs ((30), (39)), ((40), (41)), and ((42, (43)), we can obtain

$$\begin{aligned}
&\mathbf{W}_{11}\mathbf{U}_s = \mathbf{B}(\gamma)\mathbf{\Omega}_1\mathbf{T} \Rightarrow \mathbf{B}(\gamma)\mathbf{\Omega}_1 = \mathbf{W}_{11}\mathbf{U}_s\mathbf{T}^{-1} \\
\Rightarrow\ &\mathbf{W}_{12}\mathbf{U}_s = \mathbf{W}_{11}\mathbf{U}_s\mathbf{T}^{-1}\mathbf{\Phi}_1\mathbf{T} \Rightarrow \mathbf{T}^{-1}\mathbf{\Phi}_1\mathbf{T} = (\mathbf{W}_1\mathbf{U}_s)^{\#}\mathbf{W}_2\mathbf{U}_s \quad (53) \\
&\mathbf{W}_{21}\mathbf{U}_s = \mathbf{B}(\phi)\mathbf{\Omega}_2\mathbf{T} \Rightarrow \mathbf{B}(\phi)\mathbf{\Omega}_2 = \mathbf{W}_{21}\mathbf{U}_s\mathbf{T}^{-1} \\
\Rightarrow\ &\mathbf{W}_{22}\mathbf{U}_s = \mathbf{W}_{21}\mathbf{U}_s\mathbf{T}^{-1}\mathbf{\Phi}_2\mathbf{T} \Rightarrow \mathbf{T}^{-1}\mathbf{\Phi}_2\mathbf{T} = (\mathbf{W}_3\mathbf{U}_s)^{\#}\mathbf{W}_4\mathbf{U}_s \quad (54) \\
&\mathbf{W}_{31}\mathbf{U}_s = \mathbf{B}(\vartheta)\mathbf{\Omega}_3\mathbf{T} \Rightarrow \mathbf{B}(\vartheta)\mathbf{\Omega}_3 = \mathbf{W}_{31}\mathbf{U}_s\mathbf{T}^{-1} \\
\Rightarrow\ &\mathbf{W}_{32}\mathbf{U}_s = \mathbf{W}_{31}\mathbf{U}_s\mathbf{T}^{-1}\mathbf{\Phi}_3\mathbf{T} \Rightarrow \mathbf{T}^{-1}\mathbf{\Phi}_3\mathbf{T} = (\mathbf{W}_5\mathbf{U}_s)^{\#}\mathbf{W}_6\mathbf{U}_s \quad (55)
\end{aligned}$$

where $(\cdot)^{\#}$ stands for pseudo-inverse. Similar to (16), we define a $(3 \times L \times L)$-dimensional TWA $\mathbf{X}$, whose 2D slices ($(L \times L)$-dimensional matrix) can be represented in a pseudo-inverse form as

$$\mathbf{X}_1 = (\mathbf{W}_1\mathbf{U}_\mathbf{s})^{\#}\mathbf{W}_2\mathbf{U}_\mathbf{s} = \mathbf{T}^{-1}\mathbf{\Phi}_1\mathbf{T}, \tag{56}$$

$$\mathbf{X}_2 = (\mathbf{W}_3\mathbf{U}_\mathbf{s})^{\#}\mathbf{W}_4\mathbf{U}_\mathbf{s} = \mathbf{T}^{-1}\mathbf{\Phi}_2\mathbf{T}, \tag{57}$$

$$\mathbf{X}_3 = (\mathbf{W}_5\mathbf{U}_\mathbf{s})^{\#}\mathbf{W}_6\mathbf{U}_\mathbf{s} = \mathbf{T}^{-1}\mathbf{\Phi}_3\mathbf{T}. \tag{58}$$

Note that an $(3 \times L \times L)$-dimensional TWA $\mathbf{X}$ can be represented in a compact form as

$$\mathbf{X} = (\mathbf{D} \otimes \mathbf{H})\mathbf{W}^T, \tag{59}$$

where $\mathbf{W} = \mathbf{T}^T$, $\mathbf{H} = \mathbf{T}^{-1}$, and

$$\mathbf{D} = \begin{bmatrix} \text{diag}^{-1}(\mathbf{\Phi}_1) \\ \text{diag}^{-1}(\mathbf{\Phi}_2) \\ \text{diag}^{-1}(\mathbf{\Phi}_3) \end{bmatrix}. \tag{60}$$

As one of the methods for fitting trilinear model, trilinear alternating least squares (TALS) approach [40–42] is appealing primarily because it is guaranteed to converge monotonically but also because of its relative simplicity (no parameter to tune, and each

step solves a standard least square problem) and good performance. The basic idea behind this method for trilinear model fitting is to update a subset of parameters using least squares regression every time, while keeping the other previous parameter estimates fixed. Such an alternating projections-type procedure is iterated for all subsets of parameters until the convergence is achieved.

The cost function of the trilinear model in Eq. (59) can be represented in a Forbenius norm-type form as:

$$\min_{\mathbf{W}} \left\| \begin{bmatrix} \mathbf{X}_1 \\ \mathbf{X}_2 \\ \mathbf{X}_3 \end{bmatrix} - \begin{bmatrix} \mathbf{H}\text{diag}_1(\mathbf{D}) \\ \mathbf{H}\text{diag}_2(\mathbf{D}) \\ \mathbf{H}\text{diag}_3(\mathbf{D}) \end{bmatrix} \mathbf{W}^T \right\|_{\mathbf{F}}^2 \tag{61}$$

It follows that the conditional (while keeping $\mathbf{H}$ and $\mathbf{D}$ fixed) least squares update for $\mathbf{W}$ is

$$\mathbf{W} = \left(\begin{bmatrix} \mathbf{H}\text{diag}_1\left(\hat{\mathbf{D}}\right) \\ \mathbf{H}\text{diag}_2\left(\hat{\mathbf{D}}\right) \\ \mathbf{H}\text{diag}_3\left(\hat{\mathbf{D}}\right) \end{bmatrix}^{\#} \begin{bmatrix} X_1 \\ X_2 \\ X_3 \end{bmatrix} \right)^T. \tag{62}$$

Similarly, from the second way of slicing the 3-D data $\mathbf{Y}_l = \mathbf{W}\text{diag}_l(\mathbf{H})\mathbf{D}^T$, $l = 1, 2, \ldots, L$, the cost function can be formed as following:

$$\min_{\mathbf{D}} \left\| \begin{bmatrix} \mathbf{Y}_1 \\ \mathbf{Y}_2 \\ \vdots \\ \mathbf{Y}_L \end{bmatrix} - \begin{bmatrix} \mathbf{W}\text{diag}_1(\mathbf{H}) \\ \mathbf{W}\text{diag}_2(\mathbf{H}) \\ \vdots \\ \mathbf{W}\text{diag}_L(\mathbf{H}) \end{bmatrix} \mathbf{D}^T \right\|_{\mathbf{F}}^2. \tag{63}$$

It follows that the conditional (while keeping $\mathbf{H}$ and $\mathbf{W}$ fixed) least squares update for $\mathbf{D}$ is

$$\mathbf{D} = \left(\begin{bmatrix} \mathbf{W}\text{diag}_1(\mathbf{H}) \\ \mathbf{W}\text{diag}_2(\mathbf{H}) \\ \vdots \\ \mathbf{W}\text{diag}_L(\mathbf{H}) \end{bmatrix}^{\#} \begin{bmatrix} \mathbf{Y}_1 \\ \mathbf{Y}_2 \\ \vdots \\ \mathbf{Y}_L \end{bmatrix} \right)^T. \tag{64}$$

Finally, from the third way of slicing the 3-D data $\mathbf{Z}_l = \mathbf{D}\text{diag}_l(\mathbf{W})\mathbf{H}^T$, $l = 1, 2, \ldots, L$, the cost function can be formed as following:

$$\min_{\mathbf{H}} \left\| \begin{bmatrix} \mathbf{Z}_1 \\ \mathbf{Z}_2 \\ \vdots \\ \mathbf{Z}_L \end{bmatrix} - \begin{bmatrix} \mathbf{D}\text{diag}_1(\mathbf{W}) \\ \mathbf{D}\text{diag}_2(\mathbf{W}) \\ \vdots \\ \mathbf{D}\text{diag}_L(\mathbf{W}) \end{bmatrix} \mathbf{H}^T \right\|_{\mathbf{F}}^2. \tag{65}$$

It follows that the conditional (while keeping $\mathbf{D}$ and$\mathbf{W}$ fixed) least squares update for $\mathbf{H}$ is

$$\mathbf{H} = \left(\begin{bmatrix} \mathbf{D}\text{diag}_1(\mathbf{W}) \\ \mathbf{D}\text{diag}_2(\mathbf{W}) \\ \vdots \\ \mathbf{D}\text{diag}_L(\mathbf{W}) \end{bmatrix}^{\#} \begin{bmatrix} \mathbf{Z}_1 \\ \mathbf{Z}_2 \\ \vdots \\ \mathbf{Z}_L \end{bmatrix} \right)^T . \tag{66}$$

According to Eqs. (62), (64), and (66), the matrices $\mathbf{D}$, $\mathbf{H}$, and $\mathbf{W}$ are not updated with least squares until convergence. Thus, the steering matrix $\mathbf{CA}$ can be restored as follows:

$$\mathbf{CA} = \mathbf{U_s}\hat{\mathbf{H}} \tag{67}$$

Based on Eqs. (20), (23), and (26), γ_l, ϕ_l, and ϑ_l can be given from $\mathbf{CA}$ as follows:

$$\hat{\gamma}_l = \frac{1}{M-3} \sum_{i=2}^{M-2} \angle \left(\frac{\mathbf{CA}(i+1,l)}{\mathbf{CA}(i,l)} \right), \tag{68}$$

$$\hat{\phi}_l = \frac{1}{M-3} \sum_{i=M+3}^{2M-1} \angle \left(\frac{\mathbf{CA}(i+1,l)}{\mathbf{CA}(i,l)} \right), \tag{69}$$

$$\hat{\vartheta}_l = \frac{1}{M-3} \sum_{i=2M+3}^{3M-1} \angle \left(\frac{\mathbf{CA}(i+1,l)}{\mathbf{CA}(i,l)} \right). \tag{70}$$

As shown in [8, 16], since the imperfect estimation of $(\hat{\gamma}_l, \hat{\phi}_l)$ can results in $\frac{\lambda}{2\pi d}\sqrt{\hat{\gamma}_l^2 + \hat{\phi}_l^2}$ being greater than unity especially when elevation angles are between 70° and 90°, causing the calculation of asin(.) to fail [8, 16], the conventional estimator $\text{asin}(\frac{\lambda}{2\pi d}\sqrt{\hat{\gamma}_l^2 + \hat{\phi}_l^2})$ will break down, i.e., estimation failure. In addition, note that even if the estimation successes when elevation angles are between 70° and 90°, the estimation accuracy in the region [70°, 90°] is lower than other regions [16]. Furthermore, although there is no estimation failure for the estimator $\text{acos}(-\frac{\lambda\hat{\vartheta}_l}{2\pi d})$ when elevation angles are between 0° and 20°, the estimation accuracy of the estimator $\text{acos}(-\frac{\lambda\hat{\vartheta}_l}{2\pi d})$ in the region [0°, 20°] is lower than other regions [8] (see the first experiment for details).

How to design an efficient estimator, which can: i) avoid the estimation failure and low estimation accuracy of $\text{asin}(\frac{\lambda}{2\pi d}\sqrt{\hat{\gamma}_l^2 + \hat{\phi}_l^2})$ for the region [70°, 90°] ; and ii) avoid the low estimation accuracy of

$\text{acos}\left(-\frac{\lambda\hat{\vartheta}_l}{2\pi d}\right)$ for the region $[0°, 20°]$? Note that $\sin(70°) = \cos(20°) \approx 0.9$, which provides an important clue for designing the above-mentioned estimator. Therefore, this paper combines $\text{acos}(-\frac{\lambda\hat{\vartheta}_l}{2\pi d})$ and $\text{asin}(\frac{\lambda}{2\pi d}\sqrt{\hat{\gamma}_l^2 + \hat{\phi}_l^2})$, sets the threshold 0.9, and give the new estimator by for elevation angle as follows:

$$\alpha_l = \begin{cases} \frac{1}{2}\left\{\text{acos}\left(\frac{-\lambda\hat{\vartheta}_l}{2\pi d}\right) + \text{asin}\left(\frac{\lambda}{2\pi d}\sqrt{\hat{\gamma}_l^2 + \hat{\phi}_l^2}\right)\right\} \\ \quad \text{if } \left(\left|\frac{\lambda\hat{\vartheta}_l}{2\pi d}\right| < 0.9\right) \text{ and } \left(\left|\frac{\lambda}{2\pi d}\sqrt{\hat{\gamma}_l^2 + \hat{\phi}_l^2}\right| < 0.9\right) \\ \text{acos}\left(\frac{-\lambda\hat{\vartheta}_l}{2\pi d}\right) \\ \quad \text{if } \left(\left|\frac{\lambda\hat{\vartheta}_l}{2\pi d}\right| < 0.9\right) \text{ and } \left(\left|\frac{\lambda}{2\pi d}\sqrt{\hat{\gamma}_l^2 + \hat{\phi}_l^2}\right| \geq 0.9\right) \\ \text{asin}\left(\frac{\lambda}{2\pi d}\sqrt{\hat{\gamma}_l^2 + \hat{\phi}_l^2}\right) \\ \quad \text{if } \left(\left|\frac{\lambda\hat{\vartheta}_l}{2\pi d}\right| \geq 0.9\right) \text{ and } \left(\left|\frac{\lambda}{2\pi d}\sqrt{\hat{\gamma}_l^2 + \hat{\phi}_l^2}\right| < 0.9\right) \\ \text{failure} \\ \quad \text{if } \left(\left|\frac{\lambda\hat{\vartheta}_l}{2\pi d}\right| \geq 0.9\right) \text{ and } \left(\left|\frac{\lambda}{2\pi d}\sqrt{\hat{\gamma}_l^2 + \hat{\phi}_l^2}\right| \geq 0.9\right) \end{cases}, \quad (71)$$

The related azimuth angle estimator is given as follows:

$$\beta_l = \text{atan}\left(\frac{\phi_l}{\gamma_l}\right). \quad (72)$$

3.4. Discussion

Although the total TLSA is affected by mutual coupling and the disturbances of the three subarrays are different from each other (i.e., $\xi(\gamma_l) \neq \xi(\phi_l) \neq \xi(\vartheta_l)$), a trilinear model is constructed to compensate the effect of mutual coupling on the three subarrays using some particularly selecting matrices.

After the unique invertible matrix $\mathbf{T}$ is obtained from the constructed trilinear model, the steering vector related to any source is restored. $\hat{\gamma}_l$, $\hat{\phi}_l$, and $\hat{\vartheta}_l$ obtained from the restored steering vector are related to the same source, thus the proposed algorithm avoids pairing parameters.

The estimator $\text{asin}(\frac{\lambda}{2\pi d}\sqrt{\hat{\gamma}_l^2 + \hat{\phi}_l^2})$ may fail and has low estimation accuracy in the region $[70°, 90°]$, and the estimator $\text{acos}(-\frac{\lambda\hat{\vartheta}_l}{2\pi d})$ has low estimation accuracy in the region $[0°, 20°]$. But the newly designed

estimator makes use of the advantages of these two conventional estimators and avoids their disadvantages. Hence, the proposed estimator can avoid estimation failure. For completion, Eq. (71) gives all the combinations of $\left|\frac{\lambda\hat{\vartheta}_l}{2\pi d}\right|$ and $\left|\frac{\lambda}{2\pi d}\sqrt{\hat{\gamma}_l^2+\hat{\phi}_l^2}\right|$. In fact, $\left|\frac{\lambda\hat{\vartheta}_l}{2\pi d}\right| = \left|\frac{\lambda\times(-2\pi d\cos\hat{\alpha}_l/\lambda)}{2\pi d}\right| = \cos\hat{\alpha}_l$ and $\left|\frac{\lambda}{2\pi d}\sqrt{\hat{\gamma}_l^2+\hat{\phi}_l^2}\right| = \sin\hat{\alpha}_l$. When $\cos\hat{\alpha}_l$ is greater than 0.9, $\sin\hat{\alpha}_l$ is certainly smaller than 0.9. Therefore, the possibility of $(\left|\frac{\lambda\hat{\vartheta}_l}{2\pi d}\right| \geq 0.9)$ and $(\left|\frac{\lambda}{2\pi d}\sqrt{\hat{\gamma}_l^2+\hat{\phi}_l^2}\right| \geq 0.9)$ is zero and the proposed algorithm can efficiently avoids estimation failure.

4. SIMULATION RESULTS

To verify the effectiveness of the proposed algorithm, we implement the following experiments. In the former three experiments without mutual coupling, we consider two L-shaped array with 16 elements with element spacing $d = \lambda/2$. Since some sensors are selected as auxiliary sensors in the presence of mutual coupling, we consider two L-shaped array with 25 elements in the fourth experiment.

In the first experiment, we consider a single source case ($e^{j0.2\pi k}$): elevation angle α and azimuth angle β vary from $(0^\circ, 0^\circ)$ to $(90^\circ, 90^\circ)$ with 5° increment. The snapshot number and the SNR are set to 200 and 10 dB, respectively. The received signals are polluted by zero-mean additive white Gaussian noises. We use the root mean square error (RMSE) as the performance measure. All results provided are based on 500 independent runs. For each (α, β), we conduct 500 trials, and count the estimation failure times as well as the averaged performance only from successful trials (RMSE of elevation angle estimations versus different azimuth-elevation pair for this single source). Figs. 2 and 3 give the averaged performance counted from successful trials of the estimator $\text{asin}(\frac{\lambda}{2\pi d}\sqrt{\hat{\gamma}_l^2+\hat{\phi}_l^2})$ and the corresponding failure rates (the failure times divided by 500 and then multiplied by 100), respectively. From the two figures, we can see that when the elevation angle lies in $[70^\circ, 90^\circ]$, the estimator $\text{asin}(\frac{\lambda}{2\pi d}\sqrt{\hat{\gamma}_l^2+\hat{\phi}_l^2})$ has low estimation accuracy even if the estimator successes [16]. Fig. 4 shows the averaged performance of the estimator $\text{acos}(-\frac{\lambda\hat{\vartheta}_l}{2\pi d})$. Since the estimator shows no estimation failure, all the corresponding failure rates are equivalent to zero and are not given [8]. We observe from Fig. 4 that when the elevation angle lies in $[0^\circ, 20^\circ]$, the estimator $\text{acos}(-\frac{\lambda\hat{\vartheta}_l}{2\pi d})$ does

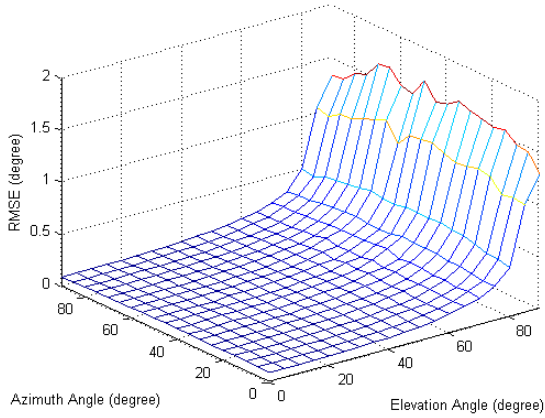

Figure 2. The averaged performance of elevation angle estimations versus different azimuth-elevation pair using the estimator $\text{asin}(\frac{\lambda}{2\pi d}\sqrt{\hat{\gamma}_l^2+\hat{\phi}_l^2})$.

not have satisfactory estimation accuracy. Fig. 5 gives the averaged performance of the proposed estimator shown in Eq. (71). The proposed estimator shows no estimation failure. In fact the proposed estimator combines the estimators $\text{asin}(\frac{\lambda}{2\pi d}\sqrt{\hat{\gamma}_l^2+\hat{\phi}_l^2})$ and $\text{acos}(-\frac{\lambda\hat{\vartheta}_l}{2\pi d})$, i.e., in the region $[0°, 20°]$, the estimator $\text{asin}(\frac{\lambda}{2\pi d}\sqrt{\hat{\gamma}_l^2+\hat{\phi}_l^2})$ is adopted; in the region $[70°, 90°]$, the estimator $\text{acos}(-\frac{\lambda\hat{\vartheta}_l}{2\pi d})$ is adopted; in the region $[20°, 70°]$, the average of $\text{acos}(-\frac{\lambda\hat{\vartheta}_l}{2\pi d})$ and $\text{asin}(\frac{\lambda}{2\pi d}\sqrt{\hat{\gamma}_l^2+\hat{\phi}_l^2})$ are adopted. Therefore, the proposed estimator shows higher estimator accuracy, and avoids estimation failure.

In the second experiment, the influence of SNR on the performance of the proposed algorithm is explored. Two uncorrelated equivalent-power sources ($e^{j0.2\pi k}$ and $e^{j0.25\pi k}$), respectively with DOA of ($\alpha_1 = 20°, \beta_1 = 20°$) and ($\alpha_2 = 40°, \beta_2 = 40°$), impinge on this array. The snapshot number is set to 400 and SNR varies from 0 dB to 30 dB. The averaged performances (RMSE of elevation and azimuth angle estimations versus SNR for two sources) and CRLB [43] over 500 Monte Carlo runs are shown in Figs. 6 and 7. From these figures, it can be seen that RMSE of the elevation and azimuth estimations decrease as SNR increases. In addition, we can see that the proposed algorithm has higher estimation accuracy than the method in [8] (by applying the pairing method in [13]).

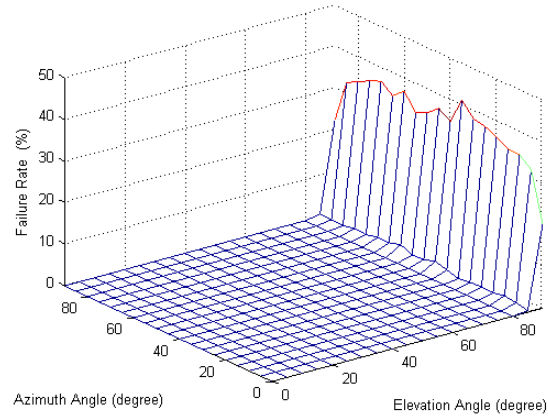

Figure 3. Failure Rates versus different azimuth-elevation pair using the estimator $\text{asin}(\frac{\lambda}{2\pi d}\sqrt{\hat{\gamma}_l^2 + \hat{\phi}_l^2})$.

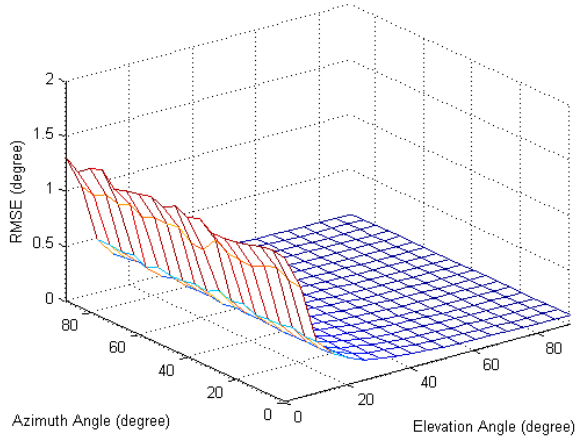

Figure 4. The averaged performance of elevation angle estimations versus different azimuth-elevation pair using the estimator $\text{acos}(-\frac{\lambda\hat{\vartheta}_l}{2\pi d})$.

In the third experiment, the same parameters as the second experiment are adopted except three sources. Three uncorrelated equivalent-power sources ($e^{j0.2\pi k}$, $e^{j0.25\pi k}$ and $e^{j0.38\pi k}$), respectively with DOAs of $(\alpha_1 = 20°, \beta_1 = 20°)$, $(\alpha_2 = 40°, \beta_2 = 40°)$, and $(\alpha_3 = 60°, \beta_3 = 60°)$ impinge on this array. The averaged performances (RMSE of elevation and azimuth angle estimations versus SNR for two

sources) over 500 Monte Carlo runs are shown in Figs. 8 and 9.

In the fourth experiment, the effect of mutual coupling on the performance of the proposed algorithm is investigated. Coupling coefficients $c_1 = 0.3527 + 0.4584i$ and $c_2 = 0.0927 - 0.1167i$. Two uncorrelated equivalent-power sources ($e^{j0.2\pi k}$ and $e^{j0.25\pi k}$), respectively with 2-D DOA of ($\alpha_1 = 20°, \beta_1 = 20°$) and ($\alpha_2 = 40°, \beta_2 =$

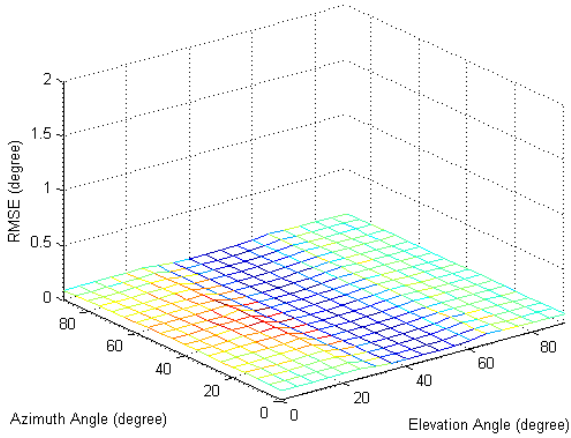

Figure 5. The averaged performance of elevation angle estimations versus different azimuth-elevation pair using the proposed estimator.

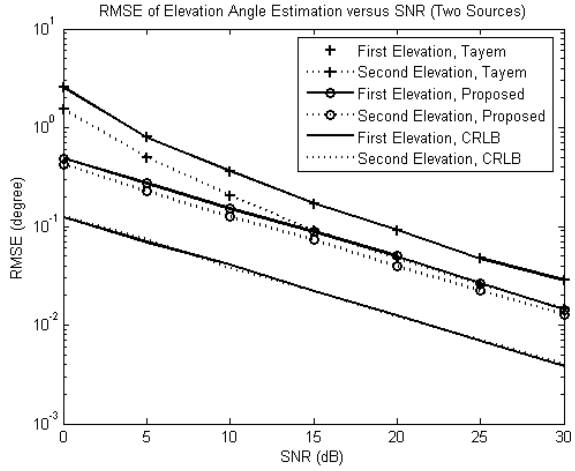

Figure 6. The averaged performance of elevation angle estimations versus SNR (two sources).

40°), impinge on this array. The number of snapshots is set to 400 and the SNR varies from 0 dB to 30 dB. The averaged performances (RMSE of elevation and azimuth angle estimations versus SNR for two sources) over 500 Monte Carlo runs are shown in Figs. 10 and 11. As it is expected, when the SNR increases, the RMSEs of the estimated

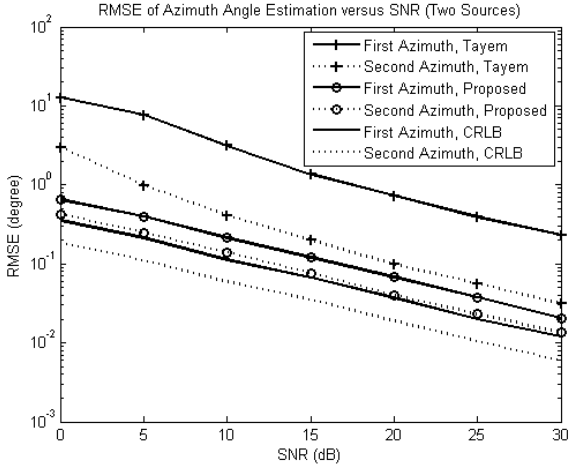

Figure 7. The averaged performance of azimuth angle estimations versus SNR (two sources).

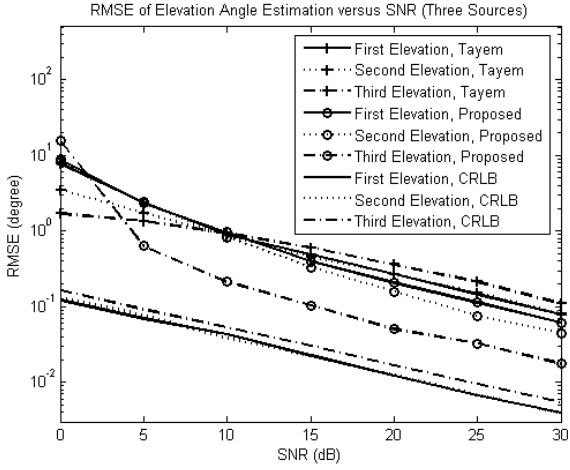

Figure 8. The averaged performance of elevation angle estimations versus SNR (three sources).

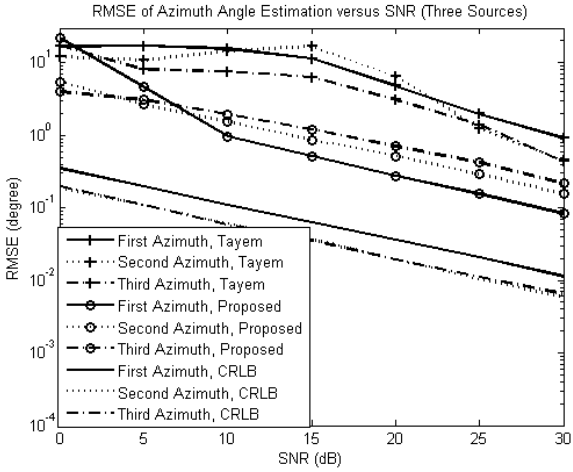

Figure 9. The averaged performance of azimuth angle estimations versus SNR (three sources).

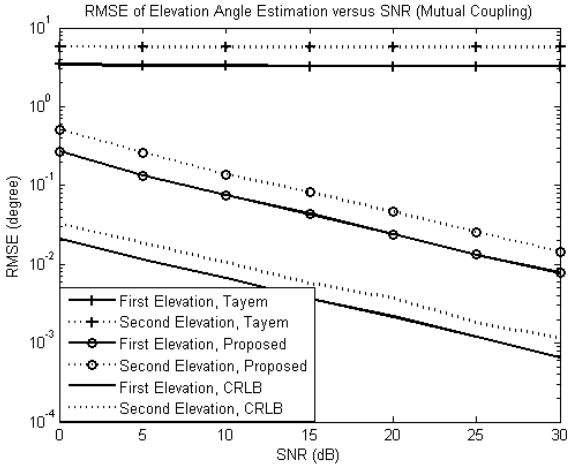

Figure 10. The averaged performance of elevation angle estimations in the presence of mutual coupling versus SNR.

parameters decrease. In addition, we observe that the proposed algorithm obviously improves the estimation accuracy compared to the methods in. [8] (applying the pairing method twice in [13] to [8]).

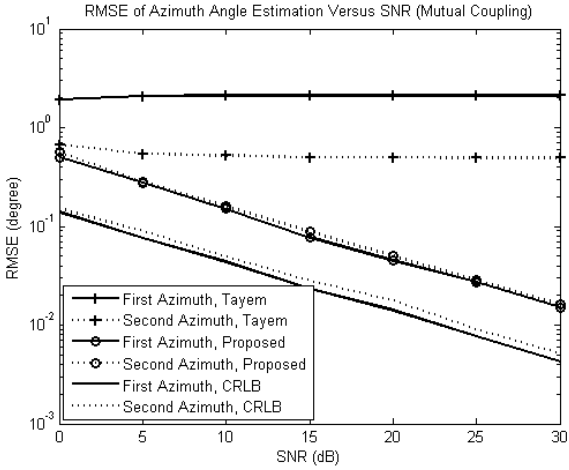

Figure 11. The averaged performance of azimuth angle estimations in the presence of mutual coupling versus SNR.

5. CONCLUSION

A new method is proposed in this paper to jointly estimate elevation and azimuth angles of multiple far-field sources in the TLSA configuration. It compensates the effect of mutual coupling, constructs a trilinear model, and restores the steering vector. From the recovered steering vector, a new elevation estimator is designed to estimate elevation angles without any matching operation or estimation failure.

ACKNOWLEDGMENT

The authors would like to thank the editor and anonymous reviewers for their valuable comments and suggestion. In addition, this work was supported by the National Natural Science Foundations of China under Grant 60901059 and 61075044, by China Postdoctoral Science Foundation funded project under Grant 201003679 and 20100481355, by the Educational Department Foundation Grant 09JK629 and Natural Science Foundation under 2010JQ8001 of Shaanxi Province, and by the Discipline Union Fund under Grant 116-210905 of Xi'an University of Technology, and the Fundamental Research Funds for the Central Universities of China Grant ZXH2010D012.

REFERENCES

1. Pillai, S. U., *Array Signal Processing*, Springer-Verlag, New York, 1989.
2. Krim, H. and M. Viberg, "Two decades of array signal processing research: The parameter approach," *IEEE Signal Process. Mag.*, Vol. 13, No. 4, 67–94, Jul. 1996.
3. Kedia, Y. S. and B. Chandna, "A new algorithm for 2-D DOA algorithm," *Signal Processing,* Vol. 60, No. 3, 325–332, Mar. 1997.
4. Zoltowski, M. D., M. Haardt, and C. P. Mathews, "Closed-form 2-D angle estimation with rectangular arrays in element space or beamspace via unitary ESPRIT," *IEEE Trans. Signal Processing*, Vol. 44, No. 2, 316–328, Feb. 1996.
5. Ramos, J., C. P. Mathews, and M. D. Zoltowski, "FCA-ESPRIT: A closed-form 2-D angle estimation algorithm for filled circular arrays with arbitrary sampling lattices," *IEEE Trans. Signal Processing*, Vol. 47, No. 1, 213–217, Jan. 1997.
6. Harabi, F., A. Gharsallah, and S. Marcos, "Three-dimensional antennas array for the estimation of direction of arrival," *IET Microwaves, Antennas and Propagation.* Vol. 3, No. 5, 843–849, 2009.
7. Hua, Y., T. K. Sarkar, and D. D. Weiner, "An L-shape array for estimation 2-D directions of wave arrival," *IEEE Trans. Antennas and Propagation*, Vol. 39, No. 2, 143–146, Feb. 1991.
8. Tayem, N. and H. M. Kwon, "L-shape 2-dimensional arrival angle estimation with propagator method," *IEEE Trans. Antennas and Propagation*, Vol. 53, No. 5, 1622–1630, May 2005.
9. Marcos, S., A. Marsal, and M. Benidir, "The propagator method for source bearing estimation," *Signal Processing*, Vol. 42, No. 2, 121–138, 1995.
10. Munier, J. and G. Y. Delisle, "Spatial analysis using new properties of the cross-spectral matrix," *IEEE Trans. Signal Processing*, Vol. 39, No. 3, 746–749, 1991.
11. Roy, R. and T. Kailath, "ESPRIT-estimation of signal parameters via rotational invariance techniques," *IEEE Trans. Acoustics, Speech, and Signal Processing*, Vol. 37, No. 7, 984–995, Jul. 1989.
12. Schmidt, R., "Multiple emitter location and signal parameter estimation," *IEEE Trans. Antennas and Propagation.* Vol. 34, No. 3, 276–280, Mar. 1986.
13. Kikuchi, S., H. Tsuji, and A. Sano, "Pair-matching method for estimating 2-D angle of arrival with a cross-correlation matrix,"

IEEE Antennas and Wireless Propagation Letters, Vol. 5, 35–40, 2006.

14. Del Rio, J. E. F. and M. F. Catedra-Perez, "The matrix pencil method for two-dimensional direction of arrival estimation employing an L-shape array," *IEEE Trans. Antennas and Propagation*, Vol. 45, No. 11, 1693–1694, Nov. 1997.
15. Shu, T., X. Liu, and J. Lu, "Comments on 'L-shape 2-dimensional arrival angle estimation with propagator method'," *IEEE Trans. Antennas and Propagation*, Vol. 56, No. 5, 1502–1503, May 2008.
16. Liu, T. H. and J. M. Mendel, "Azimuth and elevation direction finding using arbitrary array geometries," *IEEE Trans. Signal Processing*, Vol. 46, No. 7, 2061–2065, Jul. 1998.
17. Van der Veen, A. J., P. Ober, and E. F. Deprettere, "Azimuth and elevation computation in high resolution DOA estimation," *IEEE Trans. Signal Processing*, Vol. 40, No. 4, 1828–1832, Jul. 1992.
18. Van der Veen, A. J. and E. F. Deprettere, "Parallel VLSI matrix pencil algorithm for high resolution direction finding," *IEEE Trans. Signal Processing*, Vol. 39, No. 2, 383–394, Feb. 1991.
19. Krim, H. and M. Viberg, "Two decades of array signal processing research: The parameter approach," *IEEE Signal Process. Mag.*, Vol. 13, No. 4, 67–94, Jul. 1996.
20. Zoltowski, M. D. and K. T. Wong, "ESPRIT-based 2-D direction finding with a sparse uniform array of electromagnetic vector array," *IEEE Trans. Signal Processing*, Vol. 48, No. 8, 2195–2304, Aug. 2000.
21. Zoltowski, M. D. and K. T. Wong, "Closed-form eigenstructure-based direction finding using arbitrary but identical subarrays on a sparse uniform cartesian array grid," *IEEE Trans. Signal Processing*, Vol. 48, No. 8, 2205–2210, Aug. 2000.
22. Hua, Y., "A pencil-MUSIC algorithm for finding two-dimensional angles and polarizations using crossed dipoles," *IEEE Trans. Antennas and Propagation*, Vol. 41, No. 3, 370–376, Mar. 1993.
23. Li, J. and R. T. Compton, "Angle and polarization estimation using ESPRIT with a polarization sensitive array," *IEEE Trans. Antennas and Propagation*, Vol. 40, No. 5, 550–555, May 1992.
24. Veen, A., P. Ober, and E. Deprettere, "Azimuth and elevation computation in high resolution DOA estimation," *IEEE Trans. Acoust. Speech, Signal Processing*, Vol. 40, No. 7, 1828–1832, Jul. 1992.
25. Liang, J. and D. Liu, "Joint elevation and azimuth direction finding using L-shaped array," *IEEE Trans. Antennas and*

Propagation, Vol. 58, No. 6, 2136–2141, Jun. 2010.

26. Swindlehurst, A. and T. Kailath, "Azimuth/elevation direction finding using regular array geometries," *IEEE Trans. Aerosp. Electron. Syst.*, Vol. 29, No. 1, 145–156, Jan. 1993.
27. Wang, B., H. T. Hui, and S. L. Mook, "Decoupled 2D direction of arrival estimation using compact uniform circular arrays in the presence of elevation-dependent mutual coupling," *IEEE Trans. Antennas and Propagation*, Vol. 58, No. 3, 747–755, Mar. 2010.
28. Goossens, B. and H. Rogier, "A hybrid UCA-RARE/Root-MUSIC approach for 2-D direction of arrival estimation in uniform circular arrays in the presence of mutual coupling," *IEEE Trans. Antennas and Propagation*, Vol. 55, No. 3, 841–849, 2007.
29. Lin, M. and L. Yang, "Blind calibration and DOA estimation with uniform circular arrays in the presence of mutual coupling," *IEEE Antennas and Wireless Propagation Letters*, Vol. 5, No. 1, 315–318, 2006.
30. Ye, Z. and C. Liu, "2-D DOA estimation in the presence of mutual coupling," *IEEE Trans. Antennas and Propagation*, Vol. 56, No. 10, 3150–3158, 2008.
31. Liu, C., Z. Ye, and Y. Zhang, "Autocalibration algorithm for mutual coupling of planar array," *Signal Processing*, Vol. 90, No. 3, 784–794, Mar. 2010.
32. Friedlander, B. and A. J. Weiss, "Direction finding in the presence of mutual coupling," *IEEE Trans. Antennas and Propagation*, Vol. 39, No. 3, 273–284, Mar. 1991.
33. Ng, B. C. and C. M. S. See, "Sensor-array calibration using a maximum-likelihood approach," *IEEE Trans. Antennas and Propagation*, Vol. 44, No. 6, 827–835, Jun. 1996.
34. Ye, Z. and C. Liu. "On the resiliency of MUSIC direction finding against antenna sensor coupling," *IEEE Trans. Antennas and Propagation*, Vol. 56, No. 2, 371–380, 2008.
35. Liu, C., Z. Ye, and Y. Zhang, "DOA estimation based on fourth-order cumulants with unknown mutual coupling," *Signal Processing*, Vol. 89, No. 9, 1839–1843, 2009.
36. Svantesson, T., "Modeling and estimation of mutual coupling in a uniform linear array of dipoles," *Proc. Int. Conf. Acoustics, Speech, Signal Processing*, Vol. 5, 2961–2964, Mar. 1999.
37. Saventesson, T., "Mutual coupling compensation using subspace fitting," *Proc. IEEE Sensor Array and Multichannel Signal Process*, Workshop, 494–498, Mar. 2000.
38. Harshman, R. A., "Foundation of the PARAFAC procedure:

Model and conditions for an 'explanatory' multi-mode factor analysis," *UCLA Working Papers in Phonetics*, Vol. 16, 1–84, Dec. 1970.

39. Smilde, A., R. Bro, and P. Geladi, *Multi-way Analysis with Applications in the Chemical Sciences*, John Wiley & Sons Ltd., The Atrium, Southern Gate, Chichester, England, 2004.
40. Sidiropoulos, N. D., G. B. Giannakis, and R. Bro, "Parallel factor analysis in sensor array processing," *IEEE Trans. on Signal Processing*, Vol. 48, No. 8, 2377–2388, 2000.
41. Sidiropoulos, N. D., G. B. Giannakis, and R. Bro, "Blind PARAFAC Receiver for DS-CDMA systems," *IEEE Trans. Signal Processing*, Vol. 48, No. 3, 810–823, 2000.
42. Sidiropoulos, N. D., COMFAC: Matlab code for LS fitting of the complex PARAFAC model in 3-D, 1998, http://www.telecom.tuc.gr/∼nikos.
43. Kay, S. M., *Fundamentals of Statistical Signal Processing: Estimation Theory*, Prentice Hall, Upper Saddle River, NJ, 1993.